# Electrostatic precipitation of dust in the Martian atmosphere: Implications for the utilization of resources during future manned exploration missions



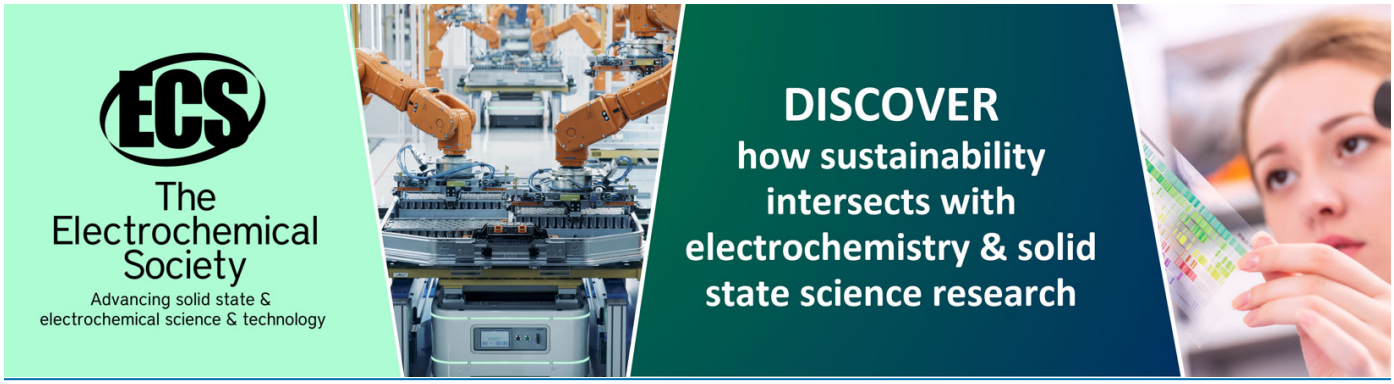

# Electrostatic precipitation of dust in the Martian atmosphere: Implications for the utilization of resources during future manned exploration missions

**C I Calle[1], S M Thompson[2], N D Cox[2], M R Johansen[1], B S Williams[3], M D Hogue[1], and J S Clements[2]**
[1] Electrostatics and Surface Physics Laboratory, NASA, Kennedy Space Center, FL 32899, USA
[2] Department of Physics and Astronomy, Appalachian State University, Boone, NC 28608, USA
[3] University of South Alabama, Mobile, AL 36688, USA

E-mail: carlos.i.calle@nasa.gov

**Abstract.** Future human missions to Mars will require the utilization of local resources for oxygen, fuel, and water. The In Situ Resource Utilization (ISRU) project is an active research endeavor at NASA to develop technologies that can enable cost effective ways to live off the land. The extraction of oxygen from the Martian atmosphere, composed primarily of carbon dioxide, is one of the most important goals of the Mars ISRU project. The main obstacle is the relatively large amount of dust present in the Martian atmosphere. This dust must be efficiently removed from atmospheric gas intakes for ISRU processing chambers. A common technique to achieve this removal on earth is by electrostatic precipitation, where large electrostatic fields are established in a localized region to charge, precipitate and collect dust particles. This technique is difficult to adapt to the Martian environment, with an atmospheric pressure of about one-hundredth of the terrestrial atmosphere. At these low pressures, the corona discharges required to implant an electrostatic charge to the particles to be collected is extremely difficult to sustain and the corona easily transitions to a glow/streamer discharge, which is unsuitable for particle charging. In this paper, we report on our successful efforts to establish a stable corona under Martian simulated conditions. We also present results on dust collecting efficiencies with an electrostatic precipitator prototype that could be effectively used on a future mission to the red planet.

## 1. Introduction

Plans for the human exploration of Mars include the concept of living off the land, exploiting the planet's natural resources for fuel, water, and oxygen. One of those resources is the Martian atmosphere itself, which is composed mainly of carbon dioxide. Using simple chemical processes, these commodities can be extracted in chemical reactors. But before that can be accomplished, dust, which is always present in the atmosphere, must be removed from the atmospheric intakes.

An electrostatic precipitator (ESP) is the obvious choice for this task [1,2]. However, the low pressure of the Martian atmosphere, at 7 to 10 mbar, prevents the large electrostatic potentials

[1] To whom any correspondence should be addressed.

normally used in terrestrial electrostatic precipitators. Although the Martian atmospheric dust is expected to be electrostatically charged, effective dust collecting at relatively low potentials would require that the dust particles be charged to saturation and with the same polarity. A corona discharge that could implant this charge could do the trick, but at the low pressures of Mars, the corona easily transitions to a glow/streamer discharge as the applied voltage is increased, and which is unsuitable for this purpose. Therefore almost no studies have been performed on low pressure $CO_2$ ESPs with the exception of Pang et al [3] who reported results for a non-customary ESP-type system using a discharge wire *external* to a tube or torus to collect dust settling out of the Martian atmosphere onto a solar panel.

In this paper, we report on our efforts to design a traditional wire-cylinder electrostatic precipitator system that could sustain a charging corona for the challenging Martian atmospheric environment. We also present data on particle charging and dust collection with this precipitator design.

## 2. Living Off the Land: In-Situ Resource Utilization

NASA's In Situ Resource Utilization (ISRU) project seeks to use space resources to reduce the mass, cost, and risk of space exploration. The specific goals of the ISRU project for Mars are to greatly reduce the expense of a human mission to the planet and to help establish the self-sufficiency of long-duration manned bases. The major areas of the Mars ISRU project are: Mission consumable production (propellants, fuel cell reagents, life support consumables, and feedstock for manufacturing and construction), surface construction (radiation shields, landing pads, and habitats), manufacturing and repair, and space utilities and power [4].

A recent evaluation of ISRU technologies recommends the continuation of the Mars atmospheric gas processing methods that are currently at a relatively high level of development [5]. These methods for mission consumable production on Mars will require the collection of dust-free Martian atmospheric gas for processing. The electrostatic precipitator reported here is being designed to efficiently remove dust from the intakes feeding the atmospheric gas processing chambers.

## 3. The Martian Atmospheric Environment

### *3.1 The dusty atmospheric environment*

The surface of Mars is entirely covered with dust with a similar composition and size throughout the planet due to its constant redistribution during global dust storms and localized dust devils. These dust storms and dust devils uplift dust into the rarefied atmosphere (Fig 1). Calculations based on optical instrumentation on spacecraft in orbit around Mars and on rovers on the surface have yielded estimates for the average diameter of dust particles in the atmosphere. Using this data, Landis *et al* believe that Martian atmospheric dust has a three-component particle size distribution: *Atmospheric dust* suspended for long periods of time, with radii ranging from 1 to 2 μm, with an average value of 1.5 ± 0.2 μm; *settled dust*, raised into the atmosphere by wind and dust devils, with a radii under 5 μm; and *saltating particles*, with radii greater than 40 μm [6].

### *3.2 Electrical properties of the Martian atmosphere*

As will be shown in detail in Section 4, atmospheric dust removal with an electrostatic precipitator requires the establishment of an electric potential difference between two metallic conductors. However, the composition and low pressure of the Martian atmosphere greatly limits the potentials that can be sustained for any length of time. At the 7 to 10 mbar atmospheric pressure, Townsend avalanche breakdown occurs at relatively low potentials [7].

In Townsend breakdown, an electron can appear in the electric field region between two electrodes as a result of a cosmic ray particle knocking it from the cathode or ionizing a gas molecule. This electron is accelerated in the electric field and is able to ionize another molecule in the gas, releasing another electron. These two electrons, in turn, are accelerated by the field, further ionizing additional molecules, and creating an avalanche of electrons accelerating toward the anode while the heavier ions

just generated accelerate toward the cathode. When the ions reach the cathode, additional *secondary electrons* are ejected in the collision. These new electrons create their own avalanches, creating a new cycle.

**Figure 1**. A dust devil photographed by the Spirit rover [Courtesy NASA]

If the electric field is weak, the number of electrons in each cycle decreases, and the charged particles that periodically appear recombine in the electrodes. In a strong field, however, the number of electrons in each cycle increases and, as a result, the avalanches increase, filling the space between electrodes with electric charges, and expanding the avalanche region. When the entire space between the electrodes becomes ionized, gap breakdown takes place.

The breakdown voltage in Townsend breakdown for a uniform electric field depends on the product of gap length $d$ and gas density. This relationship is known as a Paschen's law [8]. Historically, the gas pressure $p$ at standard temperature is plotted instead of gas density, but these curves must be adjusted for the low temperature regions on Mars. Breakdown experiments with uniform fields have been performed for most elemental and molecular gases, including $CO_2$. Note that voltage polarity is usually not reported because it does not matter when using identical (symmetric) electrodes that are far from a ground plane. In 2004, we performed experiments with a premixed gas to emulate the Martian atmosphere, composed of a mixture of 95% carbon dioxide, 2.7% nitrogen, 1.6% argon, 0.13% oxygen, and 0.07% carbon monoxide [9]. Data was taken at pressures ranging from 270 mbar to 466 mbar (200 mtorr to 350 torr) with gaps of 5 mm, 7.5 mm, and 10 mm. Fig. 2 shows that breakdown potentials in $CO_2$ and in the Martian gas mixture are extremely similar. It appears as if $CO_2$ dictates the Paschen breakdown and that the other gases, present in relatively low concentrations, do not affect it substantially. The Martian gas breakdown voltages are equal to or slightly smaller than the $CO_2$ voltages by an average of 15 volts, perhaps due to the known lower breakdown potentials of nitrogen and argon, present in smaller concentrations. Based on these results we used either a 95% $CO_2$/5% air mixture or pure $CO_2$ to approximate the Martian atmosphere in the present study.

The Mars atmospheric gas has a minimum breakdown potential of 500 V at 5 torr·mm [9]. We also obtained the same value for $CO_2$. Earlier experimental values for $CO_2$ give a potential of 420 V at 5.1 torr mm [10]. For the typical Mars atmospheric pressure of 7 mbar (5.2 torr), the breakdown potentials that we obtained in a uniform field are 725 V for a 5 mm gap, 800 V for a 7.5 mm gap, and 895 for a 10 mm gap. From our Paschen plot, we expect potentials of the order of 2.8 kV for a 10 cm gap. At the 10 mbar upper end of the Martian atmospheric pressure, these voltages range from 800 V for a 5 mm gap to 3.2 kV for a 10 cm gap in a uniform electric field.

In addition to gas breakdown, dust particle charging and migration is also affected by the low gas pressures on Mars. The roughly 100× lower gas pressure on Mars results in molecular mean free paths $\lambda$ that are ~ 100× longer than those at atmospheric pressure, e.g., for $CO_2$, $\lambda$ = 44 nm at one atmosphere [11] and ~4 μm at 5 mbar. The mean free path can be adjusted for temperature and pressure using the equations in Schmid [11] with the Sutherland constant for $CO_2$ = 220. There are three particle charging

regimes that are defined based on the Knudsen number Kn, which is simply the ratio of λ to particle radius. The regimes are continuum (Kn << 1), free molecular (Kn >> 1), and transitional (Kn ~ 1). The low pressure on Mars shifts dust particle charging from the continuum regime to the transitional. Drag on the particle as it moves through the gas is also affected. Stoke's drag is proportional to the particle radius and the gas viscosity. Although viscosity only depends on temperature and not pressure, the Stoke's formula still has to be adjusted using the Cunningham slip correction factor to account for the particle "slipping" between the gas molecules due to their large mean free paths.

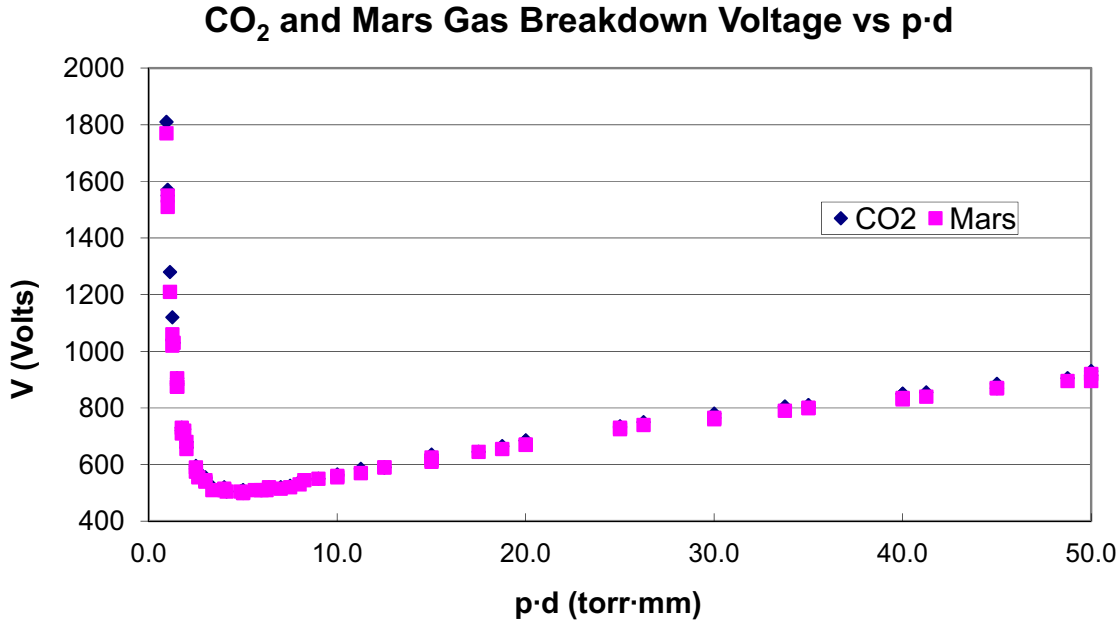


**Figure 2.** Paschen breakdown potentials versus pressure-distance for a Martian gas mixture (red squares) and for $CO_2$ (blue triangles) [9].

## 4. Precipitator Theory

An electrostatic precipitator (ESP) consists of two electrodes set at an electrostatic potential difference that can drive charged particles to one of the electrodes for collection. There are two general types of electrostatic precipitators: Single-stage or Cottrell precipitators, where particle charging and particle collection take place in a single state; and two-stage or Penney precipitators, with a pre-charging stage and a collecting stage. In both precipitator types, dust particles are charged using corona generation around the high voltage discharge electrode, which ionizes gas molecules. These ions are accelerated by the electric field $E$ in the region between the electrodes, but numerous collisions with gas molecules results in a constant drift velocity characterized by an ion mobility $b = E$/velocity. The ions transfer charge to dust particles encountered in their path as they drift to the grounded collecting electrode. The ions form space charge which modifies the applied E between the electrodes. The electric field for a wire-cylinder geometry without space charge is given by:

$$E(r) = \frac{V}{r ln(\frac{R}{a})} \tag{1}$$

where $V$ is the applied voltage, $r$ is the distance from the wire, $a$ is the wire radius, and $R$ is the cylinder radius. [12] contains an equation for the case with space charge:

$$E(\mathrm{r}) = \sqrt{\frac{I}{2\pi\varepsilon_0 Lb} + \left(\frac{a}{r}\right)^2 \left\{\left(\frac{V}{a \ln\frac{R}{a}}\right)^2 - \frac{I}{2\pi\varepsilon_0 Lb}\right\}} \tag{2}$$

where $V$ is the applied voltage, $I$ is the ion current, $L$ is the length of the wire-cylinder, $R$ is the cylinder radius, $a$ is the wire radius and $b$ is the ion mobility. Larger ion currents yield more space charge with increases the applied electric field substantially.

Since the atmospheric gas intakes for the ISRU processing chambers will likely be cylindrical, we chose a cylindrical precipitator geometry (Fig. 3). When the voltage between the electrodes is raised gradually, the glow of the corona appears in the inner electrode, where the electric field is stronger and is able to ionize the gas. The ionic current is weak and thus not able to reduce the voltage between the electrodes. When the voltage is further increased, the corona current increases with the square of the applied voltage. At higher potentials, the glowing corona envelope begins to break up into filaments that appear and disappear within a few microseconds forming a streamer corona. For our single-stage design, we are interested in obtaining the highest possible charge on the dust particles without reaching the unstable streamer corona region.

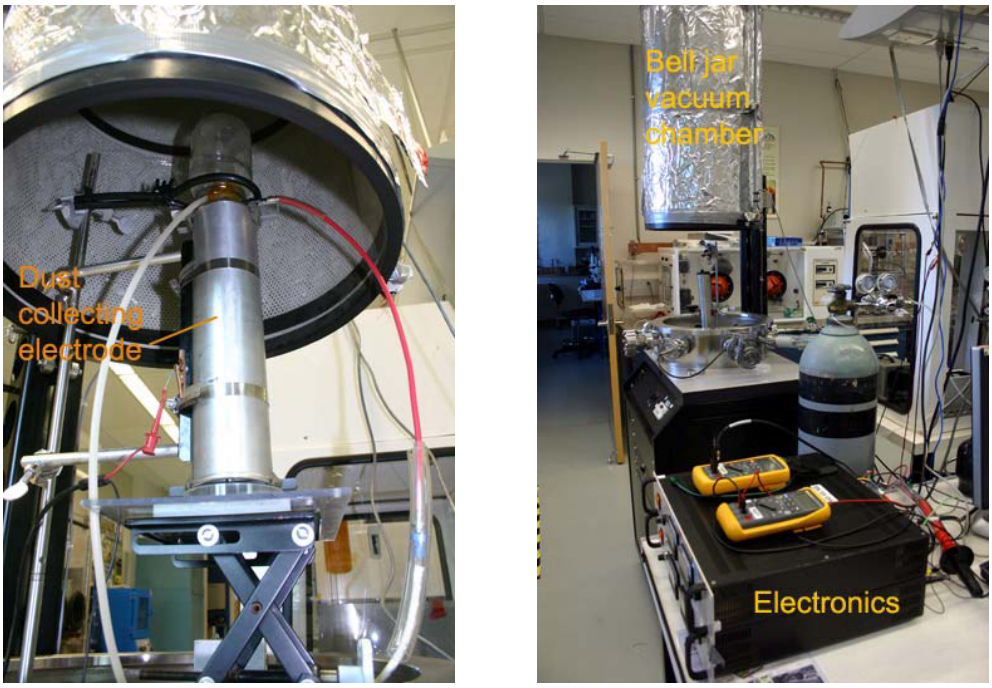


**Figure 3.** Electrostatic Precipitator assembly (left) and supporting equipment (right).

Gas ions formed by the strong electric field in a precipitator charge dust particles in two ways: *field charging* and *diffusion charging*. In field charging, the drifting ions follow the electric field lines to the dust particles. The number of possible ions attaching to the surface of a particle is clearly proportional to the square of the particle radius. The charging process continues until charge saturation $q_s$ is achieved, which takes place with a characteristic time $\tau$ given by

$$\tau = \frac{4\varepsilon_0}{N_0 e b} \tag{3}$$

where $\varepsilon_0$ is the permittivity of free space, $N_0$ is the ion number density in $m^{-3}$, e is the fundamental charge, and $b$ is the ion mobility. The particle charge as a function of time $q(t)$ is given by:

$$q(t) = q_s \frac{t}{t+\tau} \tag{4}$$

The saturation charge can be calculated from the external field and the distortion to the field by the charged particle. This calculation was first performed by Pauthenier and Moreau-Hanot [13]. Field charging is known as Pauthenier charging and is valid in the continuum regime.

The Pauthenier saturation charge for a spherical particle of radius $a$ is reached when the force due to the field $E$ and the force or repulsion from the charged particle are balanced [14]. This saturation charge is

$$Q_s = 12(k/k+2)\pi\varepsilon_0 E a^2 \tag{5}$$

where $k$ is the relative permittivity of the particle. The term $(k/k+2) = 1$ for conductive particles.

In diffusion charging, ions diffuse through the gas due to thermal motion, colliding with the dust particles at random. Technically, diffusion charging does not have a saturation limit because the charging does not stop but instead the rate slows as the particle acquires charge which repels the incoming ions. The ions have a distribution of velocities and energies, and ions with too little energy are repelled. Eventually only a very few ions in the high energy tail of the distribution can reach the particle, and the amount of additional charging becomes insignificant. The diffusion charge acquired by dust particles can be calculated using standard kinetic theory of gases. This charge depends on the ion number density, $N_0$, their mean velocity, $c_i$, and the cross sectional area of the particle, $\pi a^2$. Cross [9] reports the expression developed by Arent [15] in the continuum regime for the diffusion charge $q$ as a function of time t

$$q(t) = \frac{4\pi\epsilon_0 kT}{\mathrm{e}} \ln\left(\frac{aN_0\,\mathrm{e}^2 c_i t}{4\epsilon_0 kT} + 1\right) \tag{6}$$

where $k$ is Boltzmann's constant, and $T$ is the temperature of the gas.

The mean ion velocity $c_i$ for $CO_2$ at 9 mbar (7 torr) and 273 Kcan be calculated from kinetic theory using the following expression [16]

$$c_i = \left(\frac{8RT}{\pi M}\right)^{\frac{1}{2}} = 362\ \mathrm{m/s} \tag{7}$$

where $R$ is the universal gas constant and $M$ the molecular mass of $CO_2$. The ion number density $N_0$ can be calculated using the relationships

$$N_0 = \frac{J}{ebE} \tag{8}$$

$$J = I/A \tag{9}$$

where $J$ is the current density, $I$ is the measured current flowing from the corona wire to the ground electrode, and $A$ is the area the current flows through. The ion number density $N_0$, half way between the electrodes for the cylindrical precipitator geometry with a typical potential difference of 1.7 kV, is $4.4 \times 10^{13}$ ions/m$^3$.

At a pressure of 1 atm, field charging dominates for particle sizes above 10 μm and diffusion charging dominates below 1 μm (Fig. 4). The region between requires a theory which incorporates both mechanisms at the same time [17,18], but simply adding the two is a fair approximation. As stated in Section 2.1, the diameters of particles in the Martian atmosphere range from 2 to 10 μm. In this case, both field and diffusion charging contribute to the charging mechanism, with field charging contributing more to the charge of the larger particles uplifted into the atmosphere during dust storm and dust devil activity, and both mechanisms contributing to the 2 to 4 μm normally found in the Martian atmosphere. Note that continuum regime theory only provides an order of magnitude estimate because transitional regime theory is more appropriate for this particle size range at Mars gas pressures. In fact, the longer mean free paths at the low Mars pressures may shift the dominant diffusion charging size range to larger dust particles. Unfortunately, transitional regime theory is quite

complicated and several different ones, all requiring numerical solution, have been proposed in the literature [19-21].

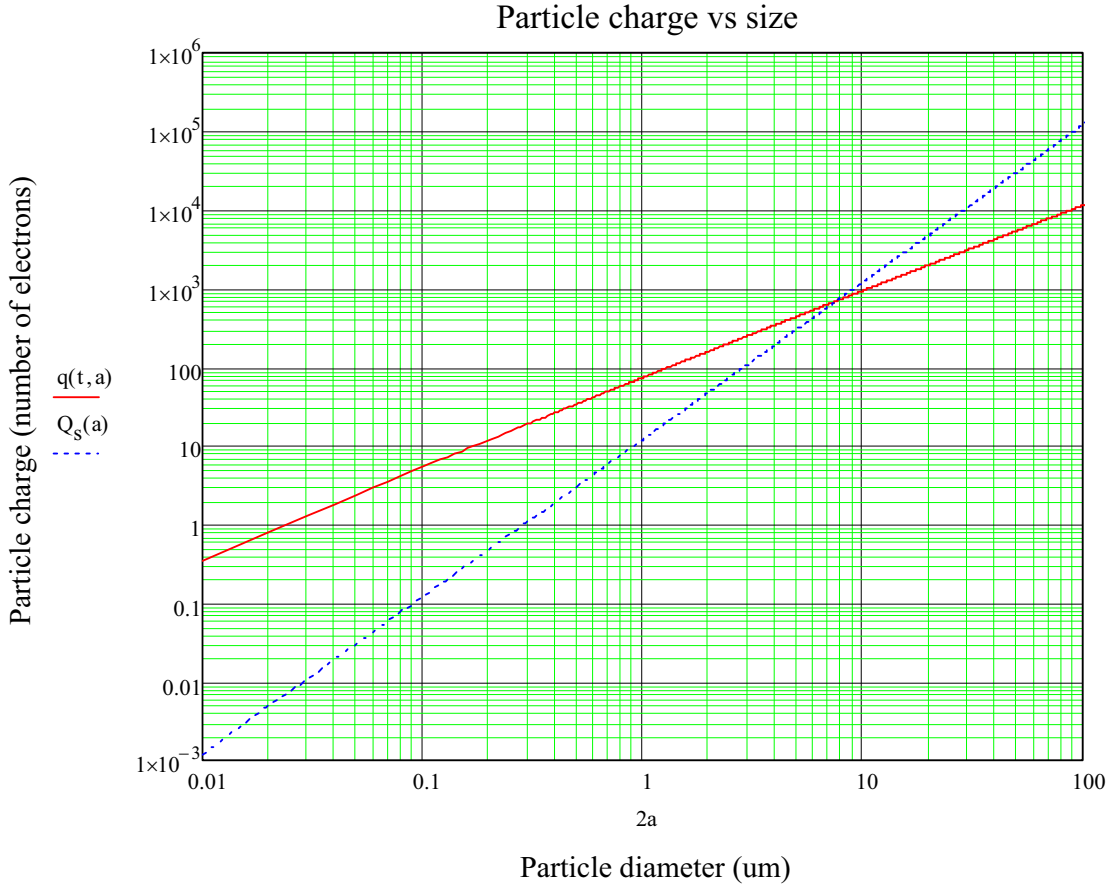


**Figure 4.** Continuum regime field (Pauthenier) saturation charge (dotted line) and diffusion charge (red line) for particles in $CO_2$ at 9 mbars with $E$ = 0.23 kV/cm and an exposure time of 10s, as given by equations (3) and (4).

Once the dust particles are charged to a level $q$, they experience an $F = qE$ force which drives them to the collecting electrode. They drift towards the electrode with a terminal velocity (migration velocity) determined by the gas drag. In the Stoke's regime (Reynold's number less than one), the drag force is given by Stoke's law with the Cunningham slip correction factor $C_c$ required for small Knudsen numbers, ie., when the particle size is not much greater than the gas molecule mean free path [16]. The migration velocity $w$ is given by [13,16]

$$w = C_c \frac{qE}{6\pi\eta a} \tag{10}$$

with

$$C_c = 1 + K_n[\alpha + \beta e^{\frac{-\gamma}{K_n}}] \tag{11}$$

where $\eta$ is the gas viscosity at that gas temperature, $a$ is the particle radius, and α,β,γ are parameters that depend on the gas composition and particle shape, etc. For $CO_2$ at STP $\eta$=1.47*$10^{-5}$, and α=1.15, β=0.479 and γ=0.92 for solid spherical particles in $CO_2$ [11]. The Knudsen number $K_n = \lambda/a$ = 8.5 for 1 μm diameter particles in the Mars atmosphere at 273 K. The Cunningham correction factor for $K_n$ = 8.5 in $CO_2$ is approximately 15. The low gas pressure on Mars increases w because of the Cunningham slip factor, but also decreases $w$ because $E$ and $q$ are limited to low values due to gas breakdown. For example, a 1 μm diameter particle in an ESP on Mars with $E$ = 0.23 kV/cm with a roughly estimated charge of about 100 electrons (see Fig. 4) would have a migration velocity $w$ = 0.4 m/s, which is higher than the typical value on Earth of 0.1 m/s for 1 μm particles [1]. For 10 um particles with 2000 electrons, $K_n$ = 0.85, and $C_c$ = 2, and w = 0.01 m/s. which is much lower than on Earth where w = 1 m/s for 10 μm particles typically. Therefore an ESP should work better than on Earth for 1 μm particles due to the very low drag for small particles only, but much worse for 10 μm particles because of the low $E$.

The precipitator collection efficiency can be estimated using the Deutsch-Anderson equation which applies to turbulent (high Reynold's number) flow in the ESP. The collection efficiency, $CE$, is given by White [1], Oglesby et al [2], and Cross [9], as

$$CE = 1 - e^{-\left(\frac{A}{V}\right)w} \tag{12}$$

where $A$ is the total collection electrode area, $V$ is the gas flow rate, and $w$ is the particle migration velocity.

The cylindrical ESP employed in our tests was oriented vertically so that in addition to the gas flow through the ESP, the dust particles settled through it due to the force of gravity. The terminal velocity of the particles occurs when the force of gravity is balanced by the Stoke' drag corrected for Cunningham slip. The equation for terminal velocity, $V_t$, is given in Hinds [16]:

$$V_t = C_c \frac{\rho d g}{18\eta} \tag{13}$$

where $\rho$ is the particle density and g is the gravitational strength. Mars dust has a density of approximately 2300 kG/$m^3$ and the strength of gravity is 0.38 of Earth's g. Using the previous values for a dust particle with 1 μm diameter, $C_c$ = 15 and $V_t$ = 0.0005 m/s. In the tests conducted in our lab, $V_t$ would be approximately 2.5× faster due to the stronger gravity on Earth. But these velocities are much slower than the migration velocity w calculated above. For a 10 um particle on Mars, $V_t$ = 0.007 m/s, which is almost as large as $w$. Therefore the smaller dust particles should be easier to collect in our vertical ESP with downward gas flow, whereas the opposite is usually the case in atmospheric pressure ESPs on Earth [1,2].

## 5. Current-Voltage Characteristics

Three 30 cm-long aluminium cylinders with inner diameters of 5.2 cm, 7.1 cm, and 9.5 cm, a 0.3-cm rod, and two steel wires with 70 μm and 100 μm in diameter were used for the outer and inner electrodes of the precipitator. All nine combinations were tested in a vacuum chamber evacuated to 5 mbars of carbon dioxide pressure.

Current-voltage ($I$-$V$) curves were obtained for seven geometries at 5 mbars in $CO_2$ and in 95% $CO_2$-5% air mixture, to approximate more closely the Martian atmospheric composition (Figs. 5 and 6). Negative corona, which is normally more stable than positive in atmospheric pressure air, yielded very steep $I$-$V$ curves (not shown) with a narrow region of stability. More importantly, the negative corona only occurred on one location on the discharge wire, and turned into a streamer with a slight increase in voltage. In contrast, positive polarity resulted in a very uniform glow on the entire wire and had a much wider stable voltage range. Because a stable, uniform corona discharge is required for effective particle charging, only positive polarity was used. In addition, a 100 MΩ high voltage 10 W resistor was added in series with the high voltage power supply to help stabilize t he discharge. With the $I$-$V$ curves, voltages for corona onset and streamer corona were determined. $I$-$V$ curves for the

seven configurations are shown in Figs. 5 and 6. Fig. 5 shows that *I-V* curves for plain $CO_2$ and for the carbon dioxide-air mixture are very similar. Thus, we decided to perform our experiments in $CO_2$ rather than in the mixture. The data for the 0.3 cm rod emphasizes how different the corona discharge is at low pressures compared to one atmosphere. In contrast to the atmospheric pressure case, corona current was easily obtained at low voltages using this large diameter rod and also for a very large 1.26 cm rod (not shown).

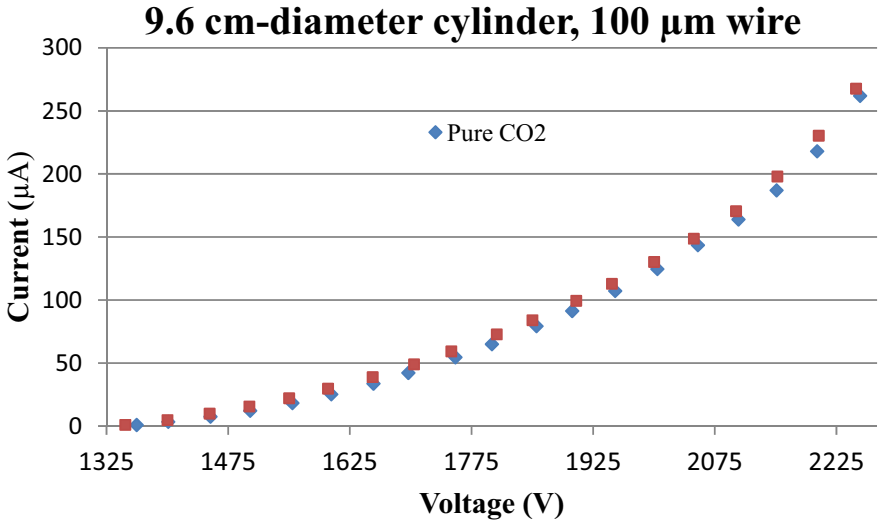


**Figure 5.** *I-V* curves for one configuration of the precipitator. Data taken at 5 mbar in pure $CO_2$ and in a 95% $CO_2$-5% air mixture, show that there is little difference in the *I-V* characteristics between the two environments at this pressure.

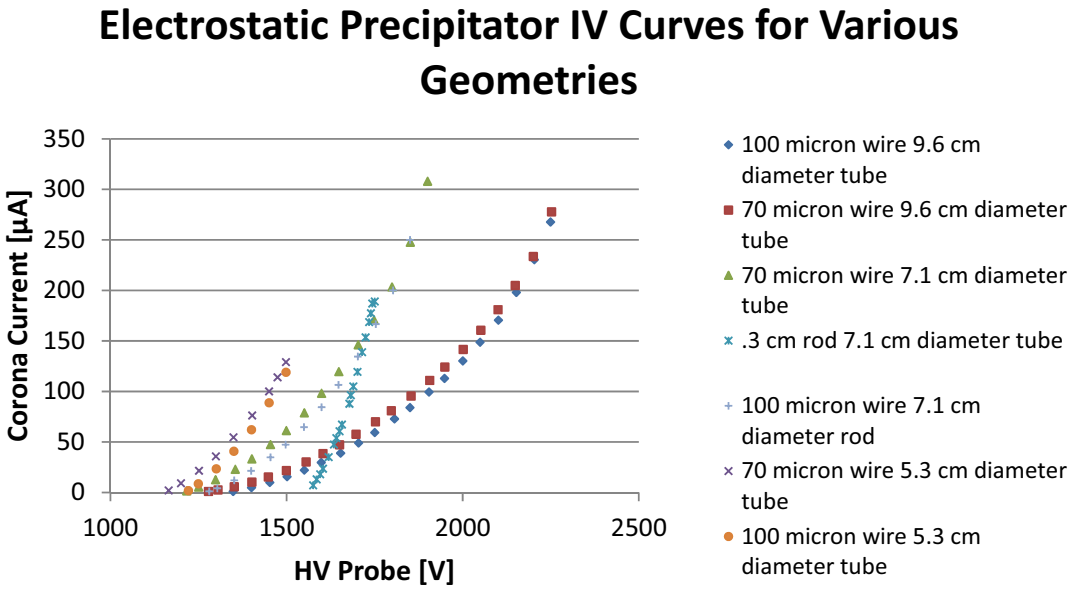


**Figure 6.** *I-V* curves for seven configurations of the precipitator. Data taken with clean electrodes and positive polarity of the wire at 5 mbar in $CO_2$.

## 6. Experiments

### *6.1 Corona Charging Experiments*

Experiments with three different brass spheres were performed to test the charging performance of the precipitator geometry in the continuum regime where Pauthenier field charging theory clearly applies. Spheres with diameters of 0.95 cm, 1.27 cm, and 2.42 cm were lowered half way into the precipitator—away from distorted edge fields—with a thin insulating Teflon thread. The thread was kept equidistant from the two electrodes and care was taken to prevent the oscillations of the thread that would alter the position of the ball. The field was turned on for 10 seconds using a DC high voltage supply. The supply was then turned off and the charged sphere was lowered into a Faraday cup connected through a coaxial vacuum feed-through to a Keithley 6514 Electrometer to obtain the value of the charge acquired by the sphere. The zero check on the electrometer was not deactivated until several seconds after the high voltage was turned off. This prevented stray ions from the corona from influencing the reading. In addition, the electrometer reading was not recorded until after the sphere was raised out of the electrometer so that the charge on the thread was not recorded. The conductive sphere was discharged when it touched the Faraday cup, which enabled the test to be repeated by simply raising the sphere back to the charging position inside the precipitator.

As indicated in Fig. 4, diffusion charging should have little effect on the charging of the brass spheres. Thus, theoretical values for field charging of the spheres using equation (3) with the electric field calculated halfway between the wire and cylinder to compare to the experimental values obtained. Table 1 shows the results for spheres of three different sizes in the 7 cm diameter cylinder with a 100 μm wire. The average of ten tests (charge measurements) and the resulting standard deviation is shown for each condition. Most of the measured values were larger than the theoretical ones, most likely due to upward drift of the electrometer and also the presence of the metal ball shortening the inter-electrode gap and thereby increasing the electric field which increases the Pauthenier saturation charge value. The ball charge data for the 7 cm cylinder with 100 um wire and 0.95 cm ball is plotted vs *E* field in Figure 7 left side. The right side of Figure 7 has a plot of charge vs the square of the ball radius at $E$ = 0.28 kV/cm. A best fit line is shown for each plot. The charge varies linearly with *E* and approximately with the square of the radius, as predicted by Pauthenier field charging theory.

**Table 1.** Brass Ball Charging Experiments in the 7 cm ESP with 100 μm wire at 5 mBar $CO_2$.

| Ball dia [cm] | Average Actual Voltage [V] | Current [uA] | R/2 Ion density N [$m^{-3}$] | Space Q R/2 E-field [kV/cm] | Field Saturation Charge [pC] | Average Measured Charge [pC] | Standard Deviation Charge [pC] | Percent Difference [%] |
|---|---|---|---|---|---|---|---|---|
| 0.47 | 1696 | 126 | 6.3E+13 | 0.28 | 51 | 66 | 6 | 29 |
| 0.95 | 1318 | 5 | 5.2E+12 | 0.12 | 93 | 110 | 7 | 19 |
| 0.95 | 1509 | 51 | 3.5E+13 | 0.20 | 150 | 166 | 5 | 11 |
| 0.95 | 1690 | 127 | 6.3E+13 | 0.28 | 210 | 225 | 7 | 7 |
| 1.27 | 1433 | 32 | 2.6E+13 | 0.17 | 231 | 261 | 7 | 13 |
| 1.27 | 1577 | 79 | 4.7E+13 | 0.23 | 311 | 323 | 9 | 4 |
| 1.27 | 1674 | 124 | 6.3E+13 | 0.28 | 371 | 362 | 9 | -2 |

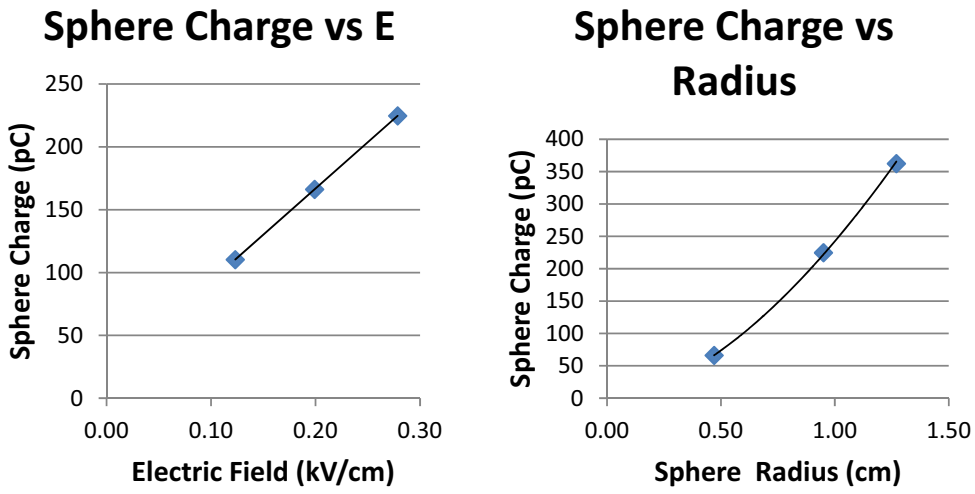


**Figure 7. Left:** Experimental values of the charge on 0.95 cm brass sphere vs *E*. **(Right):** Experimental charge at *E* = 0.28 kV/cm vs sphere radius. Data taken in the 7 cm diameter cylindrical ESP with 100 μm wire at 5 mbar in $CO_2$.

### *6.2 Precipitator Dust Experiments*

The *I-V* curves for the seven configurations shown in Fig. 6 show that both the 100 μm and the 70 μ wires with the 9.6 cm diameter tube provided the largest stable voltage range between corona onset and streamer formation, as well as a relatively wide range in the corona current available for particle charging. Since the 100 μm wire is easier to handle, we decided to start our precipitator experiments with that configuration. However, the 9.6 cm width of the tube is perhaps too large for the comparatively small potentials allowed at the low pressure in the chamber. Dust particles falling through the precipitator have a larger distance to travel to the collecting electrode, resulting in little collection. Since the 100 μm wire with the 7.0-cm diameter tube did charge the simulant dust particles, all experiments were performed with that configuration.

About 2 mg of JSC Mars-1 simulant dust particles under 35 μm in diameter were introduced into the chamber through a Tygon tube and gas feed-through. The dust was aerosolized into a 1 liter polyethylene container inside the vacuum chamber located 1 cm above the ESP with a puff of $CO_2$ gas that raised the pressure in the chamber from 8.5 mbar to 9.3 mbar. A small net gas flow entered the ESP which carried dust through the precipitator, and the dust also fell with a terminal velocity dependent on the strength of gravity and the drag force. The dust collected on a silicon wafer mirror placed 5 cm under the exit of the ESP. Tribocharging of the dust during injection with no field on was measured with a Faraday cup located below the ESP. Appropriate tube and container material selection minimized this charging process to obtain a more controlled charging process in the precipitator.

Images of the dust collected on the silicon wafer with the fields on and off were analyzed to obtain particle size distributions (PSD). Fig. 8 shows PSD data for five experiments with the field turned off. Three, five, and ten $CO_2$ gas puffs, each carrying about 2 mg of the Mars simulant that sent dust through the precipitator and collected on the wafer were examined and photographed with an optical microscope at 100× magnification. PSD data for these runs show that the largest fraction of particles lies in the under 10 μm size fraction, matching the particle size distribution expected in the Martian atmosphere.

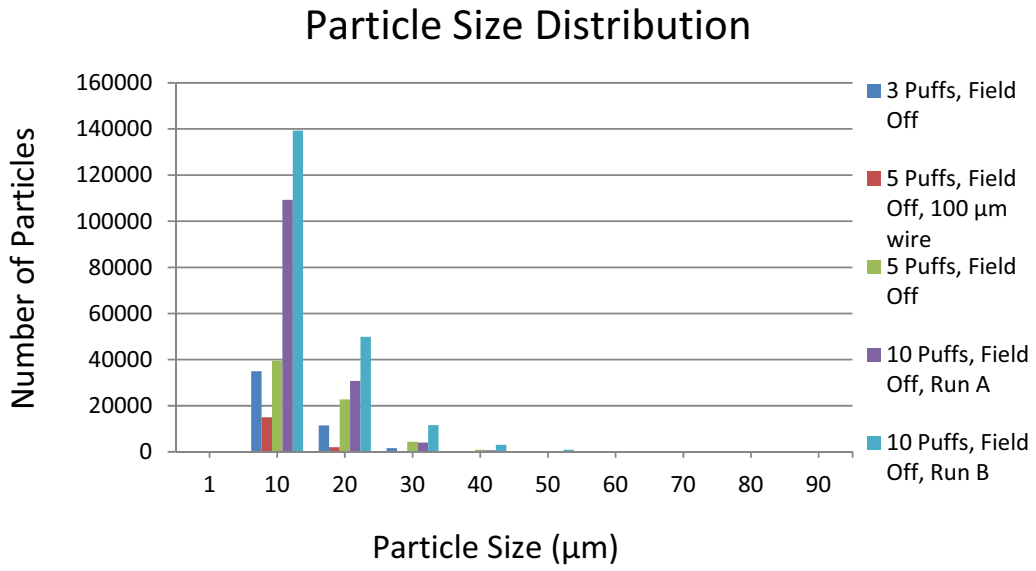


**Figure 8.** Particle size distribution of JSC Mars-1 simulant dust particles introduced into the chamber with short puffs of $CO_2$ gas and aerosolized before falling through the precipitator with the field off. Three, five, and ten puffs, each carrying about 2 mg of simulant dust, were supplied. Dust was collected on silicon wafers 7 cm in diameter. Four runs were performed with the 7.0 cm-0.3 cm rod outer-inner electrode configuration and one with the 7.0 cm-100 µm configuration. Smaller numbers of particles with diameters in the 60 to 90 µm size fractions, ranging from 1 to 309, are too small to show up on the graph.

Efforts to standardize the amount of dust introduced in the chamber are underway so that PSD data with and without the field on can be compared for quantification of ESP collecting performance. Microscope images of dust collected on the silicon wafer with and without the field on show promising performance results (Fig. 9). The applied voltage was 1600 V. No determination of possible nanoparticle production in the precipitator was made.

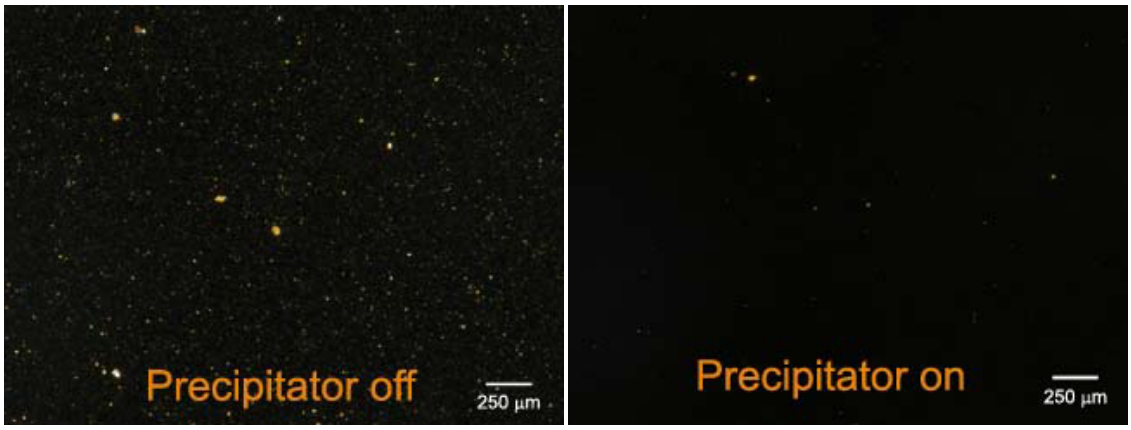


**Figure 9.** Microscope images at 100× of JSC Mars-1 dust simulant particles aerosolized in the vacuum chamber and sent through the precipitator with the field off (left) and with the potential set at 1600 V (right). The largest particles seen on the image with the field on are outside the range of particles expected in the Martian atmosphere.

It is estimated that the amount of dust in the Martian atmosphere can be as high as 2,000 particles per cubic centimeter. The Materials Adherence Experiment on the Mars Pathfinder mission provided data showing that dust deposition on surfaces averaged about 0.29% per Martian day [22]. Measurements of the visible/near infrared reflectance spectra of the radiometric calibration targets on the Mars Pathfinder rover show dust fall rates of about 20-45 μm per Earth year [23]. Figure 10 shows the Mars Exploration Rover Spirit and Opportunity Color Calibration Targets before landing and after 23 and 246 Martian days. The amount of dust deposited into the ESP will be determined by comparison to these dust deposition rates.


**Figure 10. (Left):** Clean color calibration target on Mars Exploration Rover Spirit. The target's mirror and the shadows cast on it by the Sun help scientists determine the degree to which dusty Martian skies alter the panoramic camera's perception of color. **(Center)**: Calibration target on the missions' twin rover Opportunity after 23 Martian days (sol). **Right):** Target after 346 sols. [Courtesy NASA/JPL/Cornell University]

## 7. Conclusions

Human exploration of the planet Mars will require the utilization of local resources to reduce the mass, cost, and risk of those future missions. Among the most important resources are water and oxygen, which can be extracted from the Martian atmosphere, composed mostly of carbon dioxide. Before the Martian atmospheric gas can be processed for the production of these commodities, dust particles with diameters ranging from 2 to 10 μm must be first removed.

The electrostatic precipitator design presented here removes simulated Martian dust particles in the required range in a simulated Martian atmospheric environment. The current-voltage, *I-V*, characteristic curves taken for the nine precipitator configurations at 9 mbars of pressure showed that cylindrical collecting electrode 7.0 cm in diameter with a concentric positive high voltage electrode 100 μm thick provides the best range of voltage and charging corona current.

The charge acquired by brass spheres placed in several different geometries of our precipitator design agreed fairly well with Pauthenier charging theory and showed that the precipitator produces the desired charge. This charging mechanism also contributes to the 2 to 10 μm dust particles expected in the Martian atmosphere. Diffusion charging, the second charging mechanism applicable to the dust particles, has little effect on the large brass spheres.

Mass determination as well as microscopic images and particle size distributions of dust collected on a silicon wafer placed directly below the precipitator with the field on and off showed excellent initial results. We are currently attempting to standardize the amount of Martian simulant dust introduced into the chamber to obtain quantification of precipitator performance.

**Acknowledgements**

This project was supported by NASA's ISRU project. We thank Dr. M. L. Lowder for her support of our experiments during the last phase of this project and Clara Wright for performing PSD analyses.

**References**

[1] White H J 1963 *Industrial Electrostatic Precipitation*, (Reading, MA Addison-Wesley)
[2] Olgesby S and Nichols G B 1978 *Electrostatic Precipitation* (New York,: Marcel Dekker)
[3] Pang H L, Atten P and Reboud J L 2009 *IEEE Trans. on Industry Applications* **45** No.1 50
[4] Sanders G B et al (2005) *International Lunar Conference* Toronto (Canada)
[5] Muscatello A C and Santiago-Maldonado E 2011 *Planetary and Terrestrial Mining Sciences Symposium and Space Resources Roundtable Second Joint Meeting* Ottawa (Canada)
[6] Landis G A, Herkenhoff K, Greeley R, Thompon S, Whelley P, and the MER Athena Science Team 2006 *LPS* **37** 1937
[7] Townsend J S 1914 *Electricity in Gases* (New York: Oxford University Press)
[8] Paschen F 1889 *Wied. Ann,* **37** 69
[9] Calle C I, Clements J S, Wills J and Buhler C R 2004 *NASA Technical Memorandum 2004-211535* 86
[10] Thomson J J and Thomson G P 1933 *Conduction of electricity through gases* (London: Cambridge University Press)
[11] Schmid O et al 2002 *Aerosol and Science Technology* **36** 351
[12] Kaiser K L 2005 *Electromagnetic Compatibility Handbook* (Boca Raton: CRC Press)
[13] Pauthenier M M and Moreau-Hanot M 1932 *J. Phys. Radium Ser.* 7 3 500
[14] Cross J 1987 *Electrostatics: Principles and Applications* (London: IOP Publishing)
[15] Arendt P and Kallman H 1926 *Z. Physics* **35** 421
[16] Hinds W C 1999 *Aerosol Technology* (New York: John Wiley and Sons)
[17] Smith W B and McDonald J R 1976 *J. Aerosol Sci.* **7** 151
[18] Liu B Y H and Kapadia A 1978 *J. Aerosol Science* **9** 227
[19] Romai F J and Piu D Y H 1993 *J. Aerosol Science* **23** 679
[20] Filippov A V 1993 J. Aerosol Science 24 424
[21] Marlow W H and Brock J R 1975 *J. Colloid Interface Science* **50** 32
[22] Landis G G and Jenkins P P 1997 *Proc. 26th IEEE Photovoltaic Spec. Conf.* Chicago (USA)
[23] Johnson J R et al 2003 *Icarus* **1163** 330